Computational Materials Science 181 (2020) 109571

Contents lists available at ScienceDirect

Computational Materials Science

journal homepage: www.elsevier.com/locate/commatsci

Migration behavior of tellurium in bcc iron against typical alloying elements: A first-principles study

Zheng-De Zhang[a,b], Cui-Lan Ren[a,c,*], Meng-Lu Tan[a,b], Yu-Qi Yang[a,b,d], Ya-Ru Yin[e], Chang-Ying Wang[f], Han Han[a], Ping Huai[a,d,e,*]

[a] Shanghai Institute of Applied Physics, Chinese Academy of Sciences, Shanghai 201800, China
[b] University of Chinese Academy of Sciences, Beijing 100049, China
[c] Key Laboratory of Interfacial Physics and Technology, Chinese Academy of Sciences, Shanghai 201800, China
[d] Shanghai Synchrotron Radiation Facility, Shanghai Advanced Research Institute, Chinese Academy of Sciences, Shanghai, 201800, China
[e] School of Physical Science and Technology, ShanghaiTech University, Shanghai 201210, China
[f] Changzhou Institute of Technology, Changzhou 213032, China

ARTICLE INFO

Keywords:
Fission products
Tellurium diffusion
Iron-based alloy
First-principles method
Nine-frequency model
Diffusion coefficients

ABSTRACT

The migration behavior of fission product tellurium in bcc iron is investigated by using the first-principles method. The tellurium energetically prefers to stay at the substitutional site, and strong attractive interactions between tellurium and monovacancies are found. The more introduced vacancy does not affect their migration barriers significantly. For their diffusivities in iron, it shows that the migration energy barriers of tellurium are highly affected with relatively larger atomic size of tellurium and strong binding with vacancy. Tellurium exhibits relatively higher diffusivity when compared to that of iron self-diffusion and common alloying elements in stainless steels (e.g. Cr, Mo, Nb, Ti, Al, Co, Cu, Mn, Ni, and W). This study can provide theoretical guidance to understand the vacancy-assisted lattice diffusion mechanisms for tellurium as well as typical alloy elements in iron.

1. Introduction

The molten salt reactor (MSR), identified as one of the six advanced nuclear fission reactors by Generation IV International Forum since 2002 [1], has received lots of attention worldwide. Specially, the liquid-fueled MSRs use molten fluoride salt as primary coolant and the nuclear fuel is dissolved in the salts. Therefore, the structural materials for the primary loop of MSRs will be in direct contact with the fuel. Historically, Hastelloy N (nickel-based alloy), initially designed by Oak Ridge National Laboratory (ORNL), has been recognized as the primary structural materials of MSRs due to their good high-temperature mechanical properties, good radiation resistance and especially the excellent corrosion resistance to molten salts [2]. It is also noted that the stainless steels (iron-based alloys) are also proposed as possible candidates for the structural materials of MSRs [3].

The fission products produced in the salts such as ^{89}Sr, ^{137}Cs, ^{140}Ba, ^{142}Ce, ^{144}Ce, ^{95}Zr, ^{95}Nb, ^{99}Mo, ^{103}Ru, ^{106}Ru, ^{125}Sb, ^{131}I, and ^{132}Te et al. under neutron irradiation would be big challenges for the structural materials [2,4]. According to the ORNL reports [5,6], the amount of tellurium (Te) deposited on the surfaces of structural materials over a period of 30-years would reach to $\sim 10^{19}$ *atoms/cm*^{2} and the maximum penetration depth of tellurium would be ~8 mils (~2.032 μm) from the surface [2]. It is also evidenced by experimental investigations [7,8] and theoretical studies [9] that the intergranular cracks formed in structural materials mainly raise from the diffusion of metallic fission product tellurium from alloy-salt interface into the bulk alloys, which would further result in the deterioration of the structural materials.

It is known that the migration of elements plays an important role in the kinetic processes such as precipitation, annealing, creep and corrosion et al.. The elements such as hydrogen, boron, carbon, with their small atomic sizes, generally behave as interstitials in metals. While for the transition metal solutes such as chromium, nickel and molybdenum et al., usually behave as substitutes in matrix materials. From the point view of microscopic defect kinetics, the non-metal elements such as H [10], He [11], B [12], C [13], as well as the metal solutes such as Cr [14], Mo [15], Nb [16], Ti [17], Al [16], Co [18], Cu [19], Mn [20], Ni [21], and W [16] et al. in bulk iron have been widely investigated by first-principles method or molecular dynamics simulations. Tellurium, as one of the main fission products in MSRs, their stabilities and chemical bonding in nickel-based alloys have been systematically studied

* Corresponding authors at: Shanghai Institute of Applied Physics, Chinese Academy of Sciences, Shanghai 201800, China.
E-mail addresses: rencuilan@sinap.ac.cn (C.-L. Ren), huaiping@sinap.ac.cn (P. Huai).

https://doi.org/10.1016/j.commatsci.2020.109571
Received 3 October 2019; Received in revised form 23 January 2020; Accepted 26 January 2020

recently. For example, Wang et al. [22] studied the stability of tellurium in grain boundaries (GBs), surface, as well as the bulk nickel. It showed that tellurium is energetically favorable at the substitutional site of nickel due to its large atomic size, and tellurium has significant tendency to segregate at the interfacial layer of GBs. With a diffusion energy barrier of 0.74 eV, the tellurium is relatively difficult to diffuse along Σ3 GB when compared to that of Σ9 and Σ11 GBs. Liu et al. [23] calculated the tellurium behavior in the nickel Σ5 GB. The expansion of Σ5 GB of nickel mainly arises from the relatively larger size of the tellurium atom, and strong tellurium-nickel bonds further weaken their surrounded Ni-Ni bonding, which is the main source of the Te-induced GB decohesion. Jia et al. [24] experimentally investigated the tellurium diffusion behavior in temperature ranging from 773 to 1173 K in nickel. The results showed that tellurium diffuses into nickel predominantly along GBs at temperature lower than 900 °C (1173 K), while an aggravated diffusion was found at elevated exposure temperature of 1000 °C (1273 K) via the lattice diffusion mechanism. However, there is a paucity of studies investigating the tellurium behavior, especially their diffusion properties in iron-based alloys up to now.

In this work, the migration behavior of tellurium in bcc iron is systematically studied by first-principles method combining with the Climbing Image-Nudged Elastic Band (CI-NEB) transition state method and nine-frequency model theory. The stability of tellurium, as well as their binding behavior with vacancies are initially studied. Furthermore, the solute migration properties via vacancy-assisted mechanism are addressed and the related mechanism via binding enthalpy, migration energy, correlation factor and the activation energy are also discussed. Additionally, the diffusion properties of tellurium are comprehensively compared with the common alloying elements including Cr, Mo, Nb, Ti, Al, Co, Cu, Mn, Ni, and W in austenite and ferrite stainless steels. The results help to understand the fundamental behavior of tellurium as well as the metal solutes in stainless steels.

2. Computational details and methodology

2.1. Computational details

The first-principles calculations were performed using the Vienna Ab-initio Simulation Package (VASP) [25–27] within the framework of spin-polarized density functional theory (DFT). The self-consistent Kohn-Sham equations were solved using projector augmented-wave (PAW) [28] method in which exchange-correlation function was described by spin-polarized Perdew-Burke-Ernzerh (PBE) of generalized gradient approximation (GGA) [29]. The cut-off energy of the plane waves was set to 400 eV, which was sufficient to obtain a good energy convergence that the total energy differences are about 0.01 eV compared with the higher energy cutoff results. The conjugate gradient algorithm was used to determine ions relaxations into local energy minimum with the total energies converged to 10^{-6} eV and the forces on each atom converged to less than 0.01 eV/Å. The minimum energy paths were investigated by CI-NEB method [30]. The vibrational frequencies were obtained by determining the Hessian matrix, and the zero-centered (Γ-point) frequencies were treated as the vibrational frequencies.

The 3 × 3 × 3 body-centered-cubic (bcc) supercells (54 atoms) were employed to model the bulk bcc-iron. The convergence test showed that the 4 × 4 × 4 *k*-point mesh of the Monkhorst-Pack [31] scheme was sufficient. The total energy differences were less than 0.005 eV per atom compared to that with 6 × 6 × 6 and even much denser *k*-point mesh. The optimized lattice constant and local magnetic moment of bcc iron were calculated to be 2.825 Å and 2.12 $\mu_B/atom$, respectively, which were in good agreement with the previous results of 2.825–2.86 [16,33,34] and 2.2 $\mu_B/atom$ [33] (see Table 1). Moveover, the activation energy (sum of formation, binding and migration energies, which will be seen later) of Te is calculated to be 1.90 eV and the difference with that in a larger model (4 × 4 × 4 supercells, 128 atoms) is less than 0.012 eV.

Table 1
The fundamental material parameters used in this work.

	Present work	Ref.
Lattice parameter a_0 (Å)	2.825	2.825[a], 2.834[b], 2.87[c]
Spin magnetic moment per atom μ_B	2.12	2.2[b]
Vacancy formation enthalpy H_f(eV)	2.18	2.22[a], 2.18[d], 2.0 ± 0.2[e]
Vacancy formation entropy $S_f(k_B)$	3.89	4.1[d], 2.1[f], 3.79[g], 4.14[g]
Self-diffusion correlation factor f_0	0.727	0.727[h]
Self-diffusion effective frequency $v_0^x(THz)$	4.67	4.65[a], 6[d], 4.9[i]

[a] DFT result from Wu (2016) [16].
[b] DFT result from Zhang (2015) [33].
[c] Experimental data from Kittle (2005) [34].
[d] DFT result from Messina (2014) [43].
[e] Experimental data from Deschepper (1983) [47].
[f] Pair-potential approach result from Hatcher (1979) [54].
[g] DFT result from Vesteylen (2017) [32].
[h] DFT result from Murali (2011) [42].
[i] DFT result from Domain (2005) [44].

2.2. Methodology

The dissolution energies (E_{dis}) of tellurium at interstitial and substitutional sites in iron matrix are defined to investigate their stabilities [35]:

$$E_{dis} = E_{Fe_nTe_1} - E_{Fe_n} - \frac{1}{m}E_{Te_m} \tag{1}$$

$$E_{dis} = E_{Fe_{n-1}Te_1} - \frac{n-1}{n}E_{Fe_n} - \frac{1}{m}E_{Te_m} \tag{2}$$

where $E_{Fe_nTe_1}$ is the total energy of the bulk iron with one interstitial tellurium atom. $E_{Fe_{n-1}Te_1}$ is the total energy of the system with one iron atom substituted by the tellurium atom. E_{Fe_n} is the total energy of the matrix of defect-free bcc iron with $n = 54$ atoms ($Im\bar{3}m$ space group) and E_{Te_m} is the total energy of simple trigonal tellurium with $m = 3$ atoms ($P3_221$ space group) [36].

The diffusion coefficients of element diffusion can be expressed with Arrhenius form [37]:

$$D = D_0 exp\left(-\frac{Q}{k_BT}\right) \tag{3}$$

where T is the Kelvin temperature. The pre-factor D_0 is expressed as (The details are provided in Supplementary Material, Note. 1):

$$D_0 = a_0^2 f v^* exp\left(\frac{\Delta S_f + \Delta S_b}{k_B}\right) \tag{4}$$

where a_0 is the lattice constant, is the Boltzmann constant. The correlation factor f of a defect diffusing in bcc lattice was approximated by Le Claire [38,39] and expressed as:

$$f = \frac{3\omega_3 + 3\omega_3^{'} + \omega_3^{''} - \frac{\omega_3\omega_4}{\omega_4 + F\omega_5} - \frac{2\omega_3^{'}\omega_4^{'}}{\omega_4^{'} + 3F\omega_0} - \frac{\omega_3^{''}\omega_4^{''}}{\omega_4^{''} + 7F\omega_0}}{2\omega_2 + 3\omega_3 + 3\omega_3^{'} + \omega_3^{''} - \frac{\omega_3\omega_4}{\omega_4 + F\omega_5} - \frac{2\omega_3^{'}\omega_4^{'}}{\omega_4^{'} + 3F\omega_0} - \frac{\omega_3^{''}\omega_4^{''}}{\omega_4^{''} + 7F\omega_0}} \tag{5}$$

with factor $F = 0.512$ [32]. The ω_i denotes the possible jump illustrated in the framework of nine-frequency model which will be discussed later. The jump frequency ω of solute-vacancy exchange is described by Eyring's [40] reaction rate theory:

$$\omega = v^* \exp(-E_m/k_BT) \tag{6}$$

where v^* denotes the effective frequency in terms of transition-state theory [41] and approximated by Wu [16]:

$$v^* = \frac{\prod_1^{3N} v_i^{ini}}{\prod_1^{3N-1} v_i^{sad}} \approx \frac{\prod_1^{3} v_i^{ini}}{\prod_1^{2} v_i^{sad}} \tag{7}$$

where v_i^{ini} and v_i^{sad} denote the attempt frequency of atoms in the three degrees of freedom (DOFs) in initial and saddle point states, respectively. The effective frequency is expressed as the quotient of the product of all real frequencies in the initial state and that in the saddle point state, which physically indicates how many vibration attempts of the initial structure are converted to the saddle point state every second. Usually, there are three attempt frequencies for each atom in their stably initial state. The unstable vibrational model for the atom in its saddle point exhibiting as imaginary frequency, is excluded from the product. Moreover, only the migrating atom is considered to get an approximation by ignoring the thermal expansion effect on other lattices.

In this work, the correlation factor f for iron self-diffusion is calculated to be 0.727, which is identical with the previous DFT result [42] (see Table 1). While the effective frequency v^* for iron self-diffusion is 4.67 THz, which is also in good agreement with DFT results [16,43,44], as listed in Table 1.

The vacancy formation entropy ΔS_f for bcc lattice can be computed in a similar manner with the harmonic approximation [45] and formula derivation (see Supplementary Material, Note. 2) by only considering the first and second nearest neighbor (1NN and 2NN) atoms to the vacancy:

$$\Delta S_f = \left[ln \frac{(\prod_1^3 v_i^{pure})^{20}}{(\prod_1^3 v_i^{V,1NN})^8 (\prod_1^3 v_i^{V,2NN})^{12}} \right] k_B \tag{8}$$

where v_i^{pure} is the vibrational frequencies for three DOFs of one iron atom in pure bcc iron. $v_i^{V,1NN}$ and $v_i^{V,2NN}$ are the frequencies of the 1NN and 2NN iron atoms to the vacancy in the system, respectively. The vacancy formation enthalpy in bcc iron is calculated to be 3.89 k_B, which is in consist with 3.79 k_B in $3 \times 3 \times 3$ supercells and slightly smaller than that in $4 \times 4 \times 4$ supercells (4.14 k_B) obtained by Vesteylen et al. [32] (see Table 1).

The solute-vacancy binding entropy ΔS_b for bcc lattice can be calculated from the supercells with and without defects [32] (see Supplementary Material, Note. 3). For self-diffusion case, ΔS_b is calculated to be zero.

$$\Delta S_b = \left[ln \frac{(\prod_1^3 v_i^{V})^8 (\prod_1^3 v_i^{S})(\prod_1^3 v_i^{S,1NN})(\prod_1^3 v_i^{S,2NN})^3 (\prod_1^3 v_i^{S,3NN})^3 (\prod_1^3 v_i^{S,5NN})}{(\prod_1^3 v_i^{pure})^9 (\prod_1^3 v_i^{V,sol})(\prod_1^3 v_i^{V,S,2NN})^3 (\prod_1^3 v_i^{V,S,3NN})^3 (\prod_1^3 v_i^{V,S,5NN})} \right] k_B \tag{9}$$

The activation energy Q in the Arrhenius expression of Eq. (3) includes the following three parts:

$$Q = E_m + H_f + H_b \tag{10}$$

The migration energy E_m for each migration process is expressed as:

$$E_m = E_{sad} - E_{ini} \tag{11}$$

where E_{sad} and E_{ini} are the total energies (or enthalpies) of the saddle and initial states in CI-NEB estimations, respectively.

The vacancy formation enthalpy H_f for the vacancy cluster in bulk material is defined as [46]:

$$H_f = E_{Fe_{n-y}V_y} - \frac{n-y}{n} E_{Fe_n} \tag{12}$$

where $E_{Fe_{n-y}V_y}$ is the total energy of the system containing y vacancies. The vacancy formation enthalpy of monovacancy in bcc iron is calculated to be 2.18 eV, which is in agreement with previous DFT [16,43] and experimental [47] results (see Table 1).

The binding enthalpy H_b between solute atoms (denoted as S) and vacancies (denoted as V) is defined as [48]:

$$E_b = \left(E_{Fe_{n-x-y}S_xV_y} + E_{Fe_n}\right) - \left(E_{Fe_{n-x}S_x} + E_{Fe_{n-y}V_y}\right) \tag{13}$$

where the first item is the total energy of the system containing x solute atoms and y vacancies. The third item is the total energy of the system with x solute atoms. A more negative binding enthalpy indicates more attractive interaction between the solute atom and the vacancies and vice versa. With such definition, H_b equals zero for the case of self-diffusion.

As expressed by Eq. (3), the diffusion coefficients for self/solute diffusion are in Arrhenius form with respect to the temperature. However, extensive experimental works [49–52] evidenced that there is a deviation from linearity in the neighborhood of the Curie temperature for the self/solute diffusion in bcc iron, in which the pre-factor is relatively little affected while the activation energy is generally affected due to the change of magnetization of iron. It is reported that the magnetic moments of atoms can be affected by their local environment [53]. In this work, all calculated energies mentioned above are in ferromagnetic (FM) state of iron with the frameworks of spin-polarized DFT calculations. The activation energy in paramagnetic (PM) state Q_{PM} could be estimated by:

$$Q_{PM} = \frac{Q_{FM}}{1+\alpha} \tag{14}$$

where the parameter α quantifies the variation of Q due to the change in magnetization of material and is also a species-dependent constant. α is chosen to be 0.16 and 0.10 for the situations of self-diffusion and solutes in the dilute limit [32].

3. Results and discussion

3.1. Stability of tellurium in iron

Tellurium is a semi-metallic chemical element in the oxygen group (Group 16 [VIA]). The atomic radius of tellurium is ~1.43 Å, which is much larger than the matrix element iron (~1.26 Å). As mentioned above, the lattice diffusions for metal solutes in alloy at elevated temperature are generally dominant by the vacancy-assistant mechanism. Therefore, the tellurium dissolutions at possible symmetrical sites as well as their binding with vacancies in bcc iron are initially investigated. The phonon spectrum for various occupations are also calculated to identify their stabilities. It shows that all the frequencies of atomic vibrations in both interstitial and substitutional Te-doped structures are real, which mean these structures are stable.

For tellurium as an interstitial, two typical trapping sites were considered: the tetrahedral and octahedral sites. It shows that the dissolution energies at tetrahedral and octahedral interstitial sites are 8.10 and 9.12 eV, respectively. In comparison, the dissolution energy of tellurium at substitutional site is 1.03 eV, which is significantly lower than that as interstitials, indicating that tellurium energetically prefers to occupy the substitute site in bcc iron. Such result is similar with that in nickel, the relatively larger atomic radius leads to its instability as interstitials [22,23]. For the substitutional tellurium, the possible Te-V, Te-V_2, Te-V_3, and Te_2-V clusters are considered and their most stable atomic configurations are shown in Fig. 1.

As benchmark calculations, the formation enthalpies of vacancies in bcc iron are calculated and listed in Table 2. The formation enthalpy of monovacancy in bcc iron is 2.18 eV in our calculation, which is in well agreement with the previous results of 2.16 eV by DFT method with PAW-PW91 potential [56], as well as the experimentally measured value of 2.0 ± 0.2 eV [47]. The binding enthalpies between the monovacancy and tellurium with possible separations at first nearest neighbor (1NN), 2NN and 3NN sites, corresponding to the I_1, I_2, I_3 atomic configurations, as shown in Fig. 1(a), are predicted to be −0.82, −0.21 and −0.07 eV, respectively. The negative binding enthalpies indicate that the binding of Te-V pairs are exothermic processes and the 1NN Te-V pair is the most energetically favorable one.

When the divacancy being introduced, the formation enthalpies of divacancies with their relative distances in 2NN, 1NN, 3NN, and 5NN

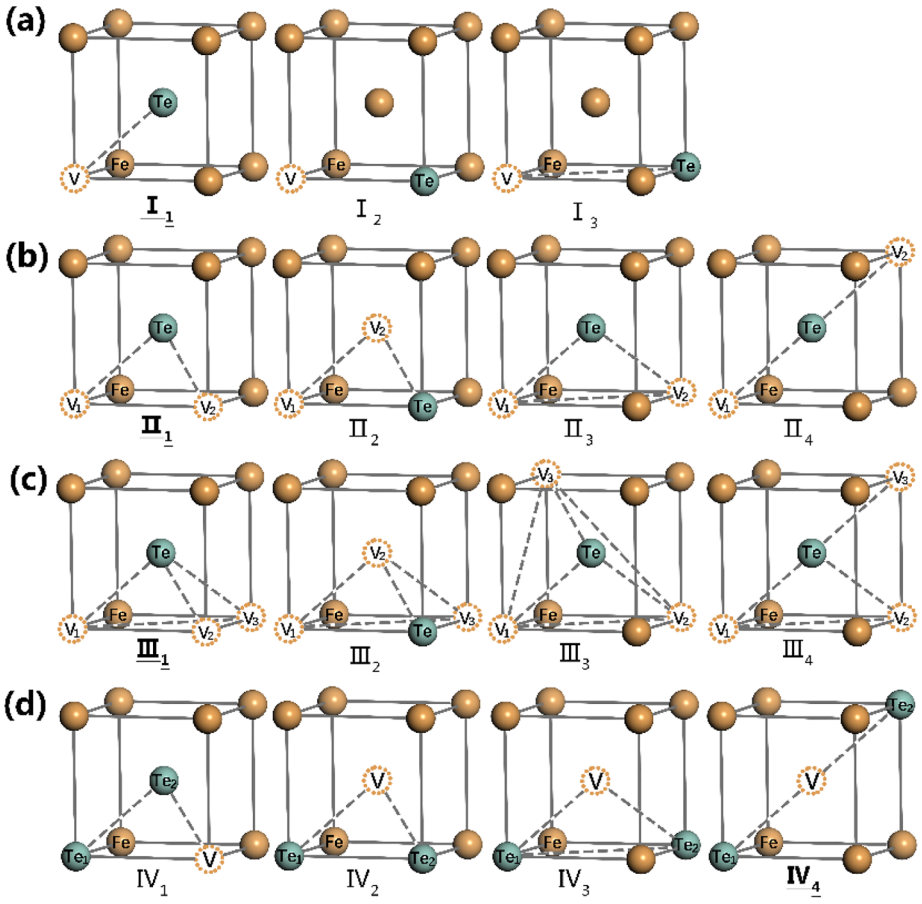

Fig. 1. The typical atomic configurations of Te_xV_y clusters in bcc iron: (a) Te-V; (b) Te-V_2; (c) Te-V_3; (d) Te_2-V.

are calculated to be 4.12, 4.18, 4.35, and 4.30 eV, respectively, which are in agreement with previous DFT calculations reported by Kandaskalov et al. [56]. With respect to the corresponding Te-V_2 clusters, the typically stable atomic configurations are II_1, II_2, II_3 and II_4, as shown in Fig. 1(b). The binding enthalpies for these Te-V_2 clusters are found to possess considerably negative values of −1.44, −1.07, −1.26, and −1.21 eV, respectively, when compared to that of Te-V pairs. It shows that the relatively compact atomic structures are much more energetically favorable by analyzing the Te-V_2 binding energies as well as their corresponding atomic configurations. The sparsity of the atomic structures can be simply identified by the sum of relative separations between tellurium and the two vacancies. For example, with respect to local structures in which two vacancies locate at 1NN sites of tellurium, the separations between two vacancies corresponds to their sparsity. The II_1 structure, with 2NN separation between two vacancies, is energetically favorable when compared to that of II_3 and II_4 with 3NN and 5NN separations. For II_1 and II_2 cases, it can be seen that the latter structure (two vacancies locate at 1NN and 2NN sites of tellurium), owns higher binding enthalpy. This indicates that vacancies like to gather around the tellurium atom. The total energies of various atomic configurations are also compared to identify their relative stability.

Various Te_2-V clusters shown in Fig. 1(d) represent the higher tellurium concentration model, in which the vacancy locates at the 1NN site of tellurium atoms. The binding enthalpies between vacancy and Te_2 with their relative distances in 1NN, 2NN, 3NN, and 5NN are

Table 2
The formation enthalpies of vacancies and their binding enthalpies with the substitutional tellurium in bcc iron. The most stable atomic configurations are shown in bold. Units are in eV.

	V_1			V_2				V_3							
				II_1	II_2	II_3	II_4	III_1	III_2	III_3	III_4				
H_f (eV)	**2.18** 1.86[a], 2.16[b], 2.0±0.2[c]			**4.12** 4.126[b]	4.18 4.136[b]	4.35 4.351[b]	4.30 4.265[b]	**6.05** 6.70[b]	6.17 6.14[b]	6.49	6.23 6.21[b]				
	Te-V_1			Te-V_2				Te-V_3				Te_2-V			
	I_1	I_2	I_3	II_1	II_2	II_3	II_4	III_1	III_2	III_3	III_4	IV_1	IV_2	IV_3	IV_4
H_b (eV)	**−0.82**	−0.21	−0.07	**−1.44**	−1.07	−1.26	−1.21	**−1.97**	−2.08	−2.15	−1.80	−0.93	−1.28	−1.64	**−1.77**

[a] Molecular dynamics (MD) result from Wang (2010) [55].
[b] DFT result from Kandaskalov (2013) [56].
[c] Experimental data from Deschepper (1983) [47].

calculated to be −0.93, −1.28, −1.64, and −1.77 eV, respectively. The tendency of binding energies clarifies that tellurium atoms do not like to be close to each other.

By comparing the general tendency of the binding enthalpy between tellurium and vacancy clusters, it shows that the binding enthalpy decreases slightly with the number of vacancies (or the tellurium atoms) increases. With the definition of vacancy formation enthalpy in Eq. (12), the formation enthalpies are in a simple exponential relation with the size of vacancy cluster [57]. And it is noted that the trivacancies with different atomic configurations possess quite large formation enthalpies among 6.05–6.49 eV when compared to the monovacancy and divacancies. Besides, the migration energy barriers for solutes via 1NN lattice jumps are approximately less than 1.35 eV, which will be discussed in the latter text.

According to Eq. (3), the diffusion coefficients for self/solute diffusion in alloys largely depends on the activation energy Q. A higher diffusion coefficient could be reached when the activation energy is lower. The activation energies consist of three parts, the vacancy formation enthalpy, the solute-vacancy binding enthalpy and the migration energy barrier, as Eq. (10) defined. Although the binding energies between Te and V_y ($y \geq 2$) clusters are usually less than that of Te-V pair, one can see that significantly increments of the formation enthalpy are found with the size of vacancy cluster increasing. It is suggested that the formation enthalpies are dominant factor to affect the activation energy when compared to that of the second and third terms by analyzing the calculated activation energies for Te_x-V_y clusters. Hence, for the further studies on the kinetic dynamic properties of those Te-V_y models, the two cases with relatively lower formation energies are selected, Te-V pair and Te-V_2 cluster, to further discuss the migration behavior of tellurium.

3.2. Te-V diffusion characters

The lattice migration processes in bcc iron are illustrated in the framework of nine-frequency model, as shown in Fig. 2(a), in which S denotes the solute or impurity atom. Among the various lattice hop processes, ω_2 denotes the migration of solute atom via 1NN vacancy site. ω_3, ω_3' and ω_3'' represent the vacancy diffuses to the iron positions which are 2NN, 3NN and 5NN sites far away from the tellurium atom, while ω_4, ω_4', and ω_4'' are their reverse diffusion processes. ω_5 is the jump process for the 2NN site vacancy to 4NN site, and ω_6 is the reverse process of ω_5. Except the above-mentioned jump processes in the solute doped model, ω_0 is defined as the self-diffusion of iron (or vacancy) in the model with absence of the solute atom.

Before going into the details, the possible solute diffusion mechanisms via solute-vacancy pair with different separations are addressed for a comparison. The detailed migration energy barriers and effective jump frequencies for various solute atoms are provided in Supplementary Material, Note. 4. Specially, the self-diffusion of iron and the diffusion of the foremost alloying element chromium are selected as typical examples to compare with the tellurium diffusion behavior. The values are listed in Table 3. The migration barrier and effective frequency for 1NN self-diffusion process (ω_0) in iron are calculated to be 0.67 eV and 4.67 THz, respectively, which are in well agreement with the previous DFT results of 0.65–0.69 eV [16,42,58] and 4.65–6 THz [16,43,44]. The migration barriers and effective jump frequencies for chromium doped iron are carefully compared with the previous DFT calculations [16]. For example, the chromium migration energy barrier and jump frequency to its 1NN vacancy site (ω_2) are 0.54 eV and 4.95 THz, respectively, which are also in good consistent with the reported results of 0.56 eV and 5.03 THz [16]. The migration barrier for tellurium diffusing to its 1NN vacancy site is 0.54 eV, which is ~ 0.13 eV lower than that of the self-diffusion of iron, indicating that the migration of tellurium is relatively easier than that of the iron self-diffusion. It should be noticed that the migration barrier of tellurium, solute chromium and iron self-diffusion are comparable, while the effective frequency of tellurium is much lower than that of chromium and iron self-diffusion. This can be attributed to the relatively lower frequencies of tellurium (3.49 THz for the third DOF as Eq. (7) defined) compared to that of chromium (5.44 THz), which may be caused by the relative larger atomic mass of tellurium.

In contrast, the 2NN self-diffusion of iron is notably difficult with much higher diffusion energy barrier of 2.59 eV from our calculation. While the diffusion energy barrier for tellurium diffusing to its 2NN vacancy site is about 2.28 eV. Such phenomenon is also reported in previous literature for chromium with 2.0 eV energy barrier for its 2NN diffusion [14]. Therefore, it is nearly impossible for metal solutes, including tellurium element, diffusing via 2NN vacancy directly, providing evidence for the previous results from *ab* initio [60] and MD simulations [61] that 1NN lattice jumps are the most frequently observed diffusion processes.

It is known that the solutes, with different atomic sizes and chemical affinities to its adjacent vacancy, would inevitably affect diffusion behavior of the nearby lattices. The migration energy barriers for various lattice jump processes are plotted in Fig. 3 and the detailed energy profiles are shown in Fig. S1 in Supplementary Material, Note. 4. Various migration processes illustrated by the nine-frequency model in Fig. 2(a) are divided into three typical situations to clarify the local effect of solutes on the lattice migrations, which is identified by different colors in Fig. 3. One is the solute/impurity diffusion process (ω_2). By taking the self-diffusion in iron as a reference, it can be seen that the migration energy barriers of ω_2 for all solutes considered in this work are all lower than that in defect-free iron matrix. Another kind of the migration processes are ω_3, ω_3', ω_3'' and ω_5, which represent the diffusion of vacancy far away from the solute atom. In another word, they are also explained as the dissociation jumps between the solute and vacancy. The migration energy barriers of ω_3, ω_3', ω_3'' and ω_5 with tellurium-doping are 1.30, 1.10, 0.98 and 0.69 eV, respectively, which are 0.63, 0.43, 0.31 and 0.02 eV higher than the situation for self-diffusion of iron. Moreover, the processes of ω_4, ω_4', ω_4'' and ω_6, which are the reverse processes of ω_3, ω_3', ω_3'' and ω_5, respectively, represent the association jumps between the tellurium and vacancy. They are relatively

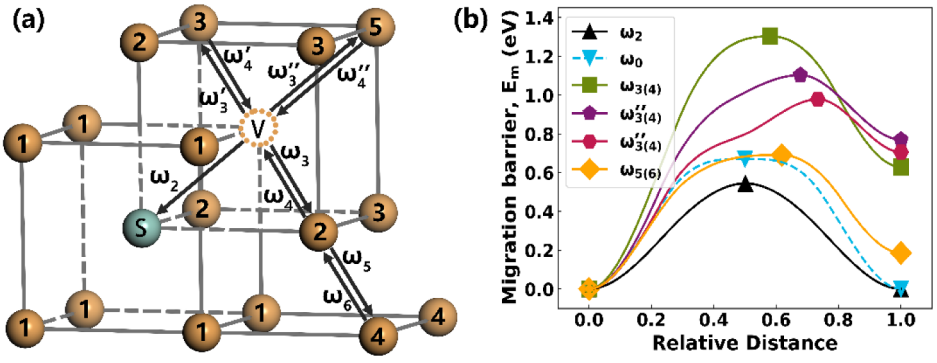

Fig. 2. (a) The illustration of the general nine-frequency model of bcc iron lattice. S denotes the solute atom, the numbers represent the relative positions of lattice iron atoms with respect to the solute atom; (b) The corresponding energy profiles for the various lattice diffusion processes in tellurium-doped model, where the reference state is 1NN Te-V pair. The scaled distances are used for these 1NN lattices jump processes.

Table 3
The effective frequencies and migration energy barriers for various lattice jumps illustrated in the nine-frequency model.

		ω_0	ω_2	ω_3	ω_3'	ω_3''	ω_5	ω_4	ω_4'	ω_4''	ω_6	ω_{2nn}
E_m (eV)	Fe	0.67 0.69[a], 0.65[b], 0.69[c], 0.55[d]										2.59
	Te		0.54	1.30	1.10	0.97	0.69	0.67	0.33	0.27	0.50	2.28
	Cr		0.54	0.67	0.67	0.62	0.72	0.63	0.61	0.60	0.68	2.34
			0.56[a]	0.69[a]	0.68[a]	0.64[a]	0.72[a]	0.65[a]	0.62[a]	0.61[a]	0.69[a]	
ν^* (THz)	Fe	4.67 4.65[a], 6[e], 4.9[f]										5.85
	Te		2.97	5.07	5.49	5.80	4.90	4.39	4.64	5.22	4.55	3.09
	Cr		4.95	4.88	4.53	4.51	4.63	4.55	4.36	4.41	4.70	7.10
			5.03[a]	4.92[a]	4.58[a]	4.57[a]	4.70[a]	4.59[a]	4.38[a]	4.44[a]	4.64[a]	

[a] DFT result from Wu (2016) [16].
[b] DFT result from Murali (2011) [42].
[c] DFT result from Soisson (2007) [58].
[d] Experimental data from Vehanen (1982) [59].
[e] DFT result from Messina (2014) [43].
[f] DFT result from Domain (2005) [44].

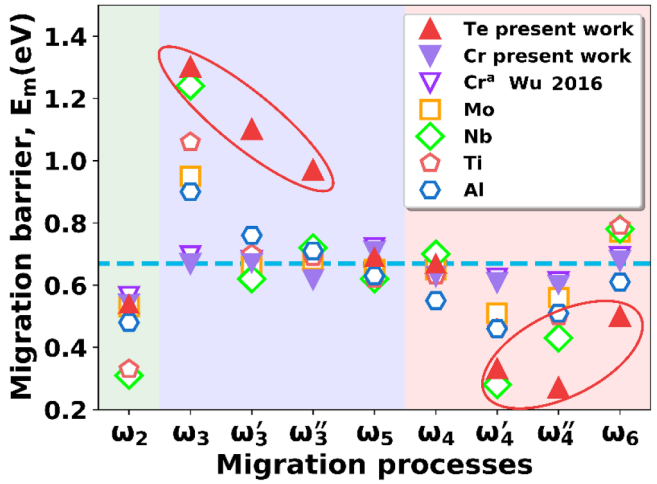

Fig. 3. The calculated migration energy barriers for Te in bcc iron based on the nine-frequency model compared to that for the general solutes including Cr, Mo, Nb, Ti, Al *etc.* The migration energy barrier for self-diffusion of iron is identified by the dashed blue line. [a]DFT result from Wu (2016) [16].

easier with comparable or smaller energy barriers corresponding to 0.67, 0.33, 0.27 and 0.50 eV, respectively. It is indicated that the pre-existing of tellurium would retards the iron atom to move closer in a large extent, in other words, the tellurium shows it's considerably affinity to vacancy. Furthermore, the lattice migrations (from ω_3 to ω_6) in tellurium-doped iron are compared with other alloying elements in ferrite stainless steels (e.g. Cr, Mo, Nb Ti, Al *etc.*), as shown in Fig. 3. It shows that among the alloying elements considered in this study, the doping of the chromium and molybdenum does not alter the lattice migration a lot, while the tellurium and niobium would significantly affect the lattice migration.

In order to more intuitively compare the tellurium behavior with other metal solutes, the binding enthalpy, migration barrier and activation energy of S-V (S denotes solute or impurity) in ferromagnetic state are summarized in Fig. 4. As shown in Fig. 4(a), the binding enthalpies between the solutes (except tellurium) and vacancy are in a range from −0.42 to 0.01 eV. The tellurium exhibits the lowest binding enthalpy of −0.82 eV, indicating its strong attractive interaction with vacancy. Additionally, the cobalt possess a positive binding enthalpy, suggesting a repulsive interaction between cobalt and vacancy, which is in agreement with previous calculation reported by Wu et al. [16]. The migration energy barriers for the metal solutes via 1NN exchanges with vacancy are shown in Fig. 4(b). It shows that the migration energy barriers for these solutes are in a range of 0.3–0.7 eV, among them a medium value of 0.54 eV is obtained for 1NN tellurium diffusion. The migration barrier of tellurium via 1NN vacancy is comparable to other alloying elements. Except Co and W, the 1NN migrations for most alloying elements considered in this study (Cr, Mo, Nb, Ti, Al, Cu, Mn and Ni) possess lower migration energy barriers, indicating that their migrations in iron are easier comparing to the iron self-diffusion. Such results are consistent with the previous results that the diffusion for most metal solutes in metal are comparable [16]. According to Eq. (10), the activation energy shown in Fig. 4(c) consist of vacancy formation enthalpy, vacancy-solute binding enthalpy and solute migration barrier. Obviously, tellurium exhibits lowest activation energy, which can be attributed to its lowest binding enthalpy. Therefore, the strong attractive interaction between tellurium and vacancy is the main reason for the rapid diffusion of tellurium in bcc iron compared with other solutes.

3.3. Solute-V2 behavior and diffusion characters

The long-distance diffusion for the solute via the vacancy-assisted migration mechanism requires alternate jump processes for solute and iron with nearby vacancies. It is reported that the long distance diffusion for a solute is difficult to be achieved via single solute-vacancy pair [14] and may need another vacancy to diffuse. According to the stability study for the different Te_x-V_y clusters shown in Section 3.1, the Te-V_2 clusters are also relatively stable. Therefore, we conceive to investigate the migration processes of solute-V_2 cluster consisting of a single solute atom (Te, Cr, Mo, Nb, Ti, Al, Co, Cu, Mn, Ni, and W) and two vacancies, in order to improve the self-vacancy-assisted migration mechanism.

As shown in Fig. 5, a multi-step net diffusion path is judiciously desired to achieve a long distance diffusion for tellurium from one primitive cell to its adjacent cell via single Te-V_2 cluster (frame (I) to frame (IX)), in which the substitutional tellurium atom and iron atom successively jump to/from their 1NN vacancy. There are various possible paths for the long-distance net diffusion, here, the following three aspects are considered to optimize the diffusion and avoid the extremely higher energy barriers. First, the initial frame of Te-V_2 cluster, in which the two vacancies (with 2NN separation) locate at the 1NN sites with respect to tellurium atom, owns lowest binding energy and is considered as the reference state for the net diffusion. Second, only the 1NN lattice exchanges for Te-V or Fe-V are adopted to avoid the much higher energy barrier via 2NN direct diffusion. Last but not least, the relatively compact atomic configurations rather than sparse ones are selected as the intermediate frames. For instance, two atomic configurations for frame (III) are selected to illustrate the importance of

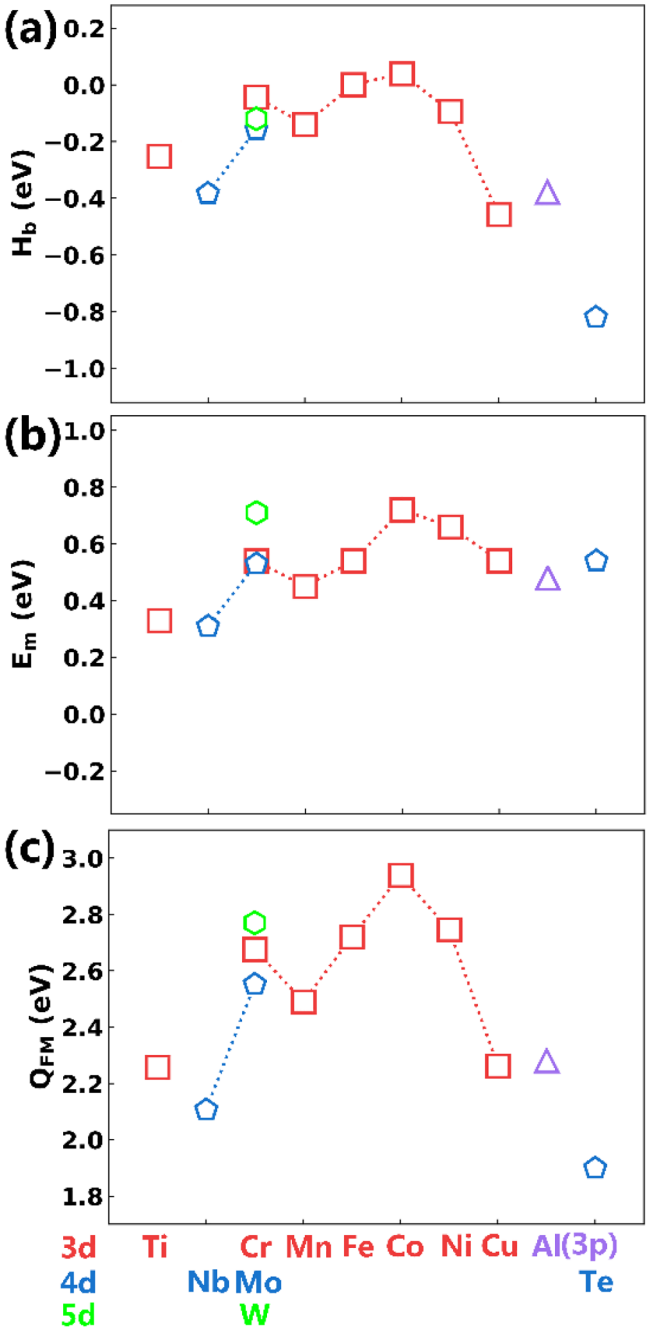

Fig. 4. (a) The binding enthalpy; (b) migration barrier; (c) activation energy in ferromagnetic state of tellurium in solute-V pair compared to alloying elements arranged by row and column of the periodic table. The 3p, 3d, 4d and 5d elements are presented by the purple triangle, red squares, blue pentagons and green hexagon, respectively.

sparsity on their stability. The frame (III_2) represents a sparser atomic structure, in which the two vacancies (2NN separation) locate at 2NN and 3NN sites of tellurium, respectively. While frame (III_1) is quite compact when compared to frame (III_1). One can see from the black dotted line shown in Fig. 6 that the total energy of frame (III_2) is 1.22 eV higher than that of frame (III_1). Moreover, the migration energy barrier for II → III_2 is also slightly higher (0.03 eV) than that for II → III_1 process. Thus, the intermediate step of III_1, with much more stable atomic structure is selected as intermediate frame.

The energy profiles for tellurium net diffusion via Te-V_2 clusters along the corresponding diffusion paths are plotted in Fig. 6 and compared with that of chromium and other alloying elements (shown in

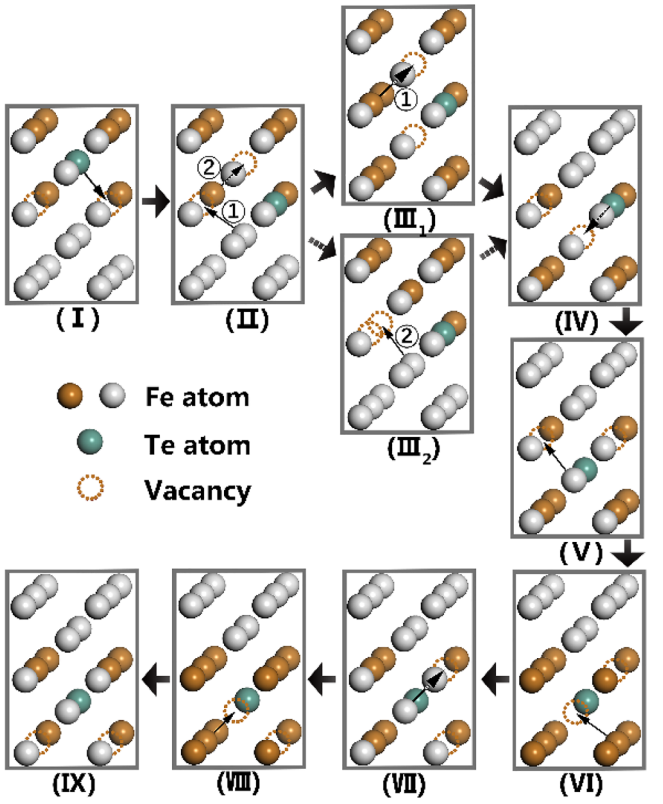

Fig. 5. The illustration of long-term net migrations of tellurium in bcc iron via Te-V_2 cluster. The tellurium atom and vacancy are denoted by the green ball and yellow-dashed circle, respectively. The cells where Te-V_2 clusters located at are represented by the dark yellow balls to guide the eye.

Fig. S2 in Supplementary Material, Note. 5). The nine frames can be divided into two categories. The total energies of frames (III), (V), (VII), and (IX) are aligned to zero with similar atomic structures to the reference frame (I), and the total energies of frames (II), (IV), (VI), and (VIII) are about 0.46 eV higher than zero point. The total energy difference arise from the inequivalence in atomic configurations, in which more intuitive atomic structures of the two categories are corresponding to the II_1 and II_2 cases in Fig. 1, respectively. A relatively lower energy is observed for the structure that the two vacancies (with 2NN separation) locates at 1NN sites with respect to tellurium atom. Therefore, for the possible Te-V_2 clusters, it also shows that the tellurium atom energetically prefers vacancies gathering around itself, as also clarified in the Section 3.1.

Among the frames illustrated in Fig. 5, the steps I → II and IV → V correspond to the tellurium diffusing into its 1NN vacancies with relative energy barriers of 0.56 and 0.12 eV, respectively. While others are the processes for iron diffusing into its 1NN vacancy sites. The absolute barrier (0.56 eV) of tellurium atom in Te-V_2 clusters is approximate to that of 1NN Te-V diffusion (0.54 eV), suggesting that further introducing vacancy does not significantly affect the 1NN tellurium migration in bcc iron. It should be mentioned that the migration barriers for tellurium and iron diffusion via Te-V_2 cluster are about 0.02 eV and 0.05 eV higher than those obtained in Te-V pair, which is in agreement with the examination on the chromium diffusion in iron previously [14]. The introducing tellurium would alter the local diffusion properties for the surrounded irons significantly. Similar results are also found in Te-V diffusions as aforementioned. The 1NN iron diffusion energy barriers vary due to different atomic configurations for the initial and final states. For example, the diffusion processes of II → III, VI → VII, and VIII → IX exhibit moderate energy barriers of 0.89 eV, in which the initial states with two vacancies (1NN separation) locate at

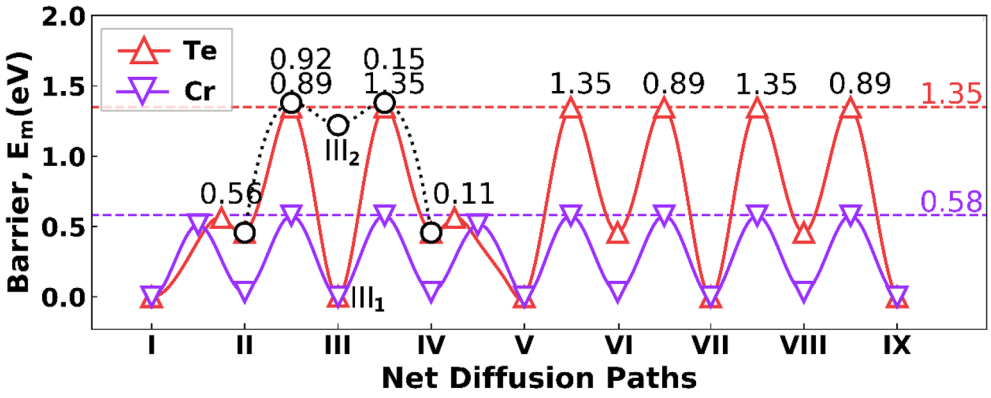

Fig. 6. Energy profiles for long distance solute diffusion via solute-V_2 cluster in bcc iron and corresponding barriers for long-term net migrations in Fig. 5. The triangles and numbers denote the absolute barriers and the relative barriers. The black dashed line represents the second path of Fig. 5(II)–(IV). The red and purple dashed line denote the max long-term migration barrier of tellurium and chromium from our calculation.

the 1NN and 2NN sites of tellurium (as the II_2 case shown in Fig. 1(b). For the processes of III → IV, V → VI, and VII → VIII, with a much lower energy for the initial state, should overcome a much higher energy barrier of 1.35 eV for further migration.

For the same net diffusion paths of Cr-V_2 cluster, as the purple dashed line shows, the maximum energy barrier for long distance migration of Cr-V_2 cluster in bcc iron are much easier with the relatively energy barrier of 0.58 eV for the possible frames considered. Such energy barrier is about 0.09 eV lower than the previous MD calculations [14]. By systematically analyzing these diffusion processes, it shows that the doping of tellurium greatly affects the surrounded lattice diffusion. As mentioned above, the doping of solute/impurity would alter the binding behavior as well as the nearby lattice diffusion properties, which can be understood by their fundamental binding behavior as follows.

The binding enthalpies and migration energy barriers for solute-V_2 are also summarized for a better comparison. The differences of binding enthalpies and migration barriers in ferromagnetic state of solutes (Te, Cr, Mo, Nb, Ti, Al, Co, Cu, Mn, Ni, and W) are shown in Fig. 7. It shows that the Te-V_2 cluster exhibits a similar binding behavior with that of Te-V pair, for which most of the metal solutes except cobalt possess negative binding enthalpies with vacancy, while the tellurium exhibits the lowest binding enthalpy among all the solutes considered in this study. As shown in Fig. 7(a), the binding enthalpy between tellurium and the two vacancies is −1.44 eV, which is much lower than that of Cr (−0.04 eV). The maximum migration barriers of niobium and tellurium are larger than other elements in Fig. 7(b). Similar to solute-V pair, the extremely lower binding enthalpy indicates the strong attraction interaction between tellurium and divacancy, which is the main reason for the higher diffusion energy barrier of tellurium when compared to other solutes.

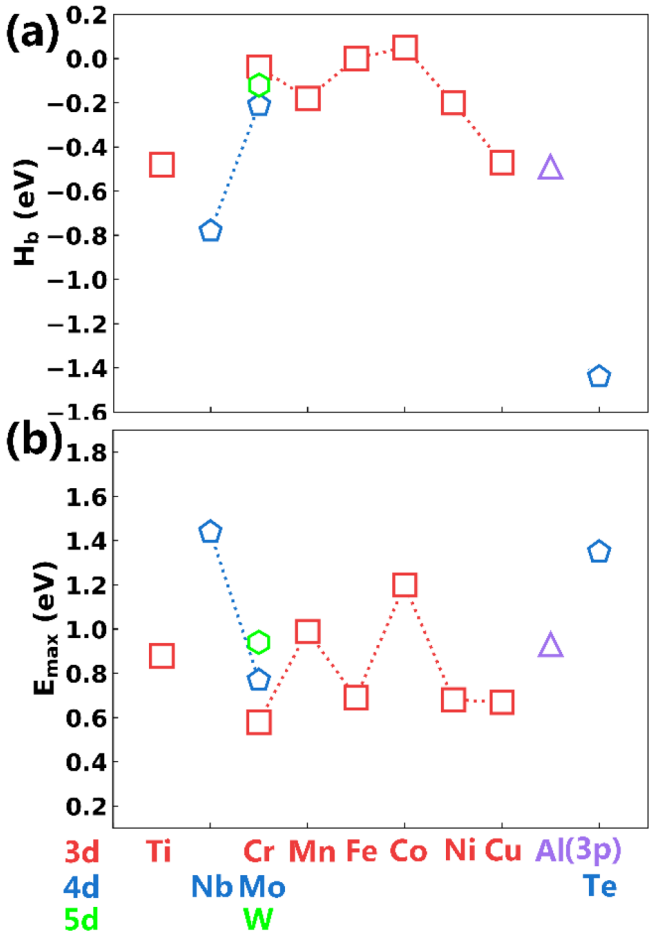

Fig. 7. (a) The binding enthalpy; (b) migration barrier in ferromagnetic state of tellurium in solute-V_2 cluster compared to alloying elements arranged by row and column of the periodic table.

3.4. Diffusivity of tellurium at finite temperature

The diffusion properties of elements in materials can be affected by temperature in a large extent. In this section, the diffusion coefficient of tellurium in bcc iron at finite temperature are evaluated from the Arrhenius diffusion equation. The parameter D_0, denoted as the pre-exponential factor or the diffusion constant, and the activation energy Q are listed in Table 4. The calculated pre-exponential factor D_0 for self-diffusion of iron is $1.33 \times 10^{-5}\ m^2/s$, which is in the same order of magnitude with the previous DFT result [32] and pair-potential approach [54]. Such value is found to be about two orders of magnitude larger than the results from the previous theoretical calculations [16,42,62], while about one order of magnitude smaller than that of the previous experimental investigation [63]. The activation energies for self-diffusion of iron in ferromagnetic state (Q_{FM}) and paramagnetic state (Q_{PM}) are calculated to be 2.85 and 2.45 eV, which agree nicely with the results obtained by Vesteylen et al. [32] and are also found to be comparable with other DFT [16,42,43,48] and experimental results [63]. When compared to the diffusion along grain boundaries in iron, the activation energy for the self-diffusion in bulk iron is much higher than that along grain boundary in iron as calculated by Inoue et al. [64] (Q = 55.7 kJ/mol, which is ~ 0.58 eV), indicating the relatively easier diffusion in pre-existed grain boundaries.

The D_0 for migration of tellurium in present work is $1.49 \times 10^{-5} m^2/s$, which is slightly larger than (and in the same order of) iron self-diffusion. Since the diffusivity of tellurium is rarely touched in the literature, we also calculate the D_0 of chromium for benchmark calculation with an order of $10^{-5} m^2/s$, which consists with the previous calculation [32]. The activation energy for tellurium in ferromagnetic state Q_{FM} is 1.90 eV, which is quite smaller than the cases of iron self-diffusion and

Table 4
The pre-exponential factor D_0 and activation energy Q for self-diffusion of iron and migration of tellurium, the values obtained in this study are shown in bold.

Element	D_0 (m^2/s)	Q_{FM} (eV)	Q_{PM} (eV)
Fe	**1.33×10^{-5}**	**2.85**	**2.45**
	3.5×10^{-5}[a]	2.830[a]	2.440[a]
	2.98×10^{-7}[b]	2.60[b]	
	5.9×10^{-7}[c]	2.66[c]	
	7.87×10^{-7}[d]	2.85[e]	
	1.6×10^{-5}[f]	2.88[g]	
	6.0×10^{-4}[h]	2.91[h]	
	2.75×10^{-3}[i]	2.63[i]	
Te	**1.49×10^{-5}**	**1.90**	**1.64**
Cr	**2.68×10^{-5}**	**2.68**	**2.44**
	7.7×10^{-5}[a]	2.732[a]	2.484[a]
	3.73×10^{-3}[j]	3.14[j]	
		2.63[e]	
Mo	5.9×10^{-5}[a]	2.650[a]	2.409[a]
Nb	7.4×10^{-5}[a]	2.560[a]	2.327[a]
Ti	7.6×10^{-5}[a]	2.656[a]	2.415[a]
	2.1×10^{-1}[k]	3.04[k]	
Al	5.0×10^{-5}[a]	2.631[a]	2.392[a]

[a] DFT result from Vesteylen (2017) [32].
[b] DFT result from Wu (2016) [16].
[c] DFT result from Murali (2011) [42].
[d] MD result from Mendelev (2009) [62].
[e] DFT result from Zhang (2014) [48].
[f] Pair-potential approach result from Hatcher (1979) [54].
[g] DFT result from Messina (2014) [43].
[h] Experimental data from Seeger (1998) [63].
[i] Experimental data from James (1966) [65].
[j] Experimental data from Lee (1990) [66].
[k] Experimental data from Klugkist (1995) [67].

all other alloying elements with the reported calculations in the range corresponding to 2.10–2.93 eV. The activation energy for tellurium and other alloying elements in paramagnetic state Q_{PM} estimated by Eq. (14) have the same tendency with that of Q_{FM}.

The Arrhenius plots of diffusion coefficients with considering their magnetic transition are shown in Fig. 8, in which the pre-factor D_0 and the activation energy Q are simply shown as the y-axis intersection and slop of the linear plot in their unitary magnetic state. As plotted in Fig. 8(a-b), the calculated diffusion coefficients of iron self-diffusion and chromium in bcc iron are in well agreement with the previous DFT calculation [32] with comparable pre-factor and the activation energy. Besides, the slopes of the iron/chromium diffusion coefficients for both FM and PM states are in well consistent with that of experimental measurements [50–52,65,66].

As shown in Fig. 8(c), the diffusion coefficients of tellurium in bcc iron are plotted and compared with that of other solutes. It shows that the diffusion coefficient of tellurium is significantly greater than other solutes in the temperature range of 700–1300 K. The diffusivities of solutes such as Cr, Mo, Nb, Ti, and Al are in an order of Nb > Ti > Al > Mo > Cr with diffusion coefficients in an order of magnitude of $\sim 10^{-19}$ m^2/s, and they all exhibit slightly better diffusivity than that of iron self-diffusion. As reported, the inlet and outlet temperature of Molten-Salt Reactor Experiment (MSRE) is 1175 to 1225 °F (908–936 K) [68]. Here, we choose the typical operating temperature of MSRE at 650 °C (923 K) as an example. The diffusion coefficient of tellurium is estimated to be 6.86×10^{-15} m^2/s, which is approximately four orders of magnitude larger than that of iron self-diffusion coefficient with 1.31×10^{-19} m^2/s, as well as Nb, Ti, Al, Mo, and Cr with corresponding values of 6.45, 2.15, 1.89, and 1.79×10^{-19} m^2/s, suggesting the fast diffusion for tellurium in bcc iron.

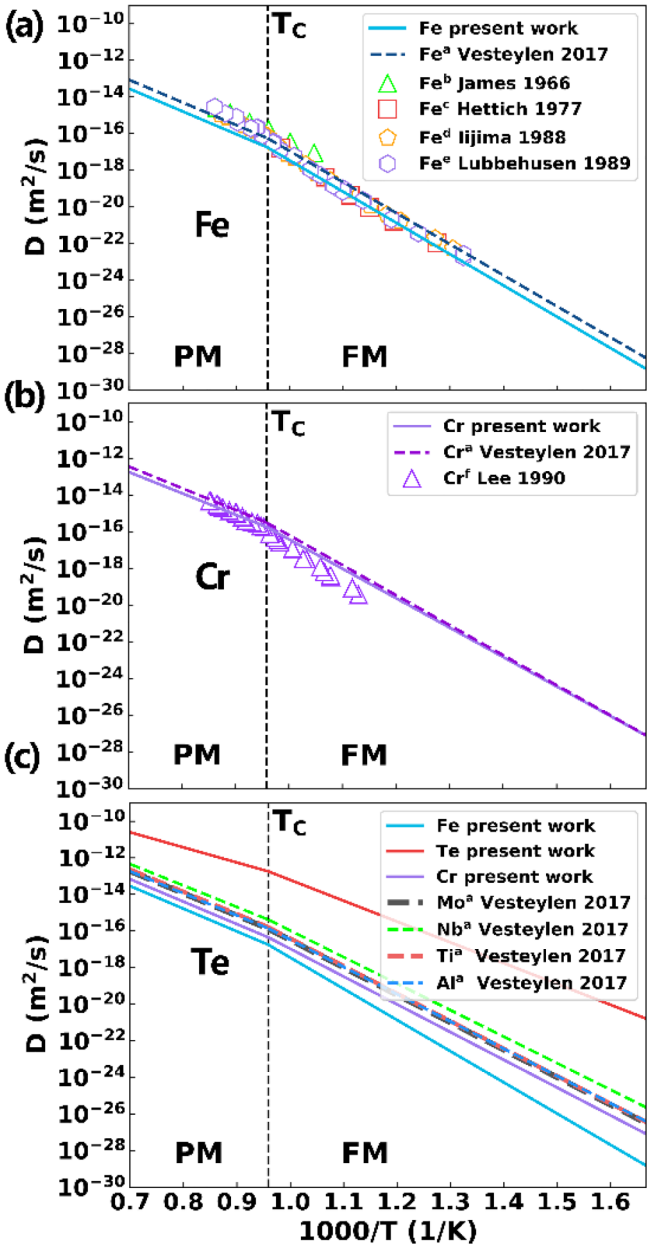

Fig. 8. Diffusion coefficients for (a) self-diffusion of iron; (b) solute chromium; (c) solute tellurium comparing to other alloying elements. The x axis is 1000 times of the inverse Kelvin temperature range from 1300 to 700 K. The Curie temperature (T_C = 1043 K) is shown in the black dotted vertical line.
[a] DFT result from Vesteylen (2017) [32].
[b] Experimental data from James (1966) [65].
[c] Experimental data from Hettich (1977) [50].
[d] Experimental data from Iijima (1988) [51].
[e] Experimental data from Lubbehusen (1989) [52].
[f] Experimental data from Lee (1990) [66].

4. Conclusion

The fundamental migration behavior of the fission product tellurium is systematically studied and compared to alloying elements in bcc iron matrix. The tellurium atom prefers to reside at the substitutional sites with the formation energy of 1.03 eV, which is much lower than that at interstitial sites (~8.10–9.12 eV). For the tellurium binding with vacancies, it is found that there is a strong attractive interaction between the tellurium and monovacancy. The long-distance net diffusion is further studied by introducing another vacancy to form solute-

divacancy cluster. The results show that further introducing vacancy does not affect the tellurium migration barriers significantly. Similar with tellurium interaction with monovacancy, the surrounded iron lattice diffusions are also significantly affected for Te-V_2 clusters when compared with other solute doping cases. The diffusion coefficients for tellurium in a temperature range of 700–1300 K are estimated via the Arrhenius equation. Tellurium exhibits relatively higher diffusivity when compared to other solutes including Nb, Ti, Al and Mo, as well as the self-diffusion of iron. The study can provide theoretical guidance to understand the vacancy-assisted lattice diffusion mechanisms for tellurium in iron.

Data availability

The raw/processed data required to reproduce these findings can be available by contacting the corresponding authors.

CRediT authorship contribution statement

Zheng-De Zhang: Methodology, Software, Validation, Formal analysis, Investigation, Data curation, Writing - original draft, Visualization. **Cui-Lan Ren:** Conceptualization, Methodology, Formal analysis, Funding acquisition, Writing - review & editing. **Meng-Lu Tan:** Software, Writing - review & editing. **Yu-Qi Yang:** Formal analysis, Writing - review & editing. **Ya-Ru Yin:** Methodology, Writing - review & editing. **Chang-Ying Wang:** Methodology, Writing - review & editing. **Han Han:** Conceptualization, Funding acquisition. **Ping Huai:** Supervision, Project administration, Methodology, Resources, Funding acquisition.

Declaration of Competing Interest

The authors declare that they have no known competing financial interests or personal relationships that could have appeared to influence the work reported in this paper.

Acknowledgments

This work was partially supported by the strategically Leading Program of the Chinese Academy of Sciences (Grant No. XDA02040100), the National Natural Science Foundation of China (Grant Nos. 11605273, 11847064 and 51901241). The authors acknowledge the TMSR Supercomputer Center and ShanghaiTech University High Performance Computing Public Service Platform for providing computing resources. The authors also thank Dr. Yan-Yan Jia from Shanghai Institute of Applied Physics for helpful discussion.

Appendix A. Supplementary data

The derivation of pre-factor D_0 and activation energy Q in Note. 1. The derivation of vacancy formation entropy ΔS_f in Note. 2. The derivation of solute-binding entropy ΔS_b for bcc lattice in Note. 3. The migration energy profiles and corresponding data for solutes (Te, Cr, Mo, Nb, Ti, Al, Co, Cu, Mn, Ni, V and W) of nine-frequency model in Note. 4. The net diffusion barrier profiles of solutes in Note. 5. Supplementary data to this article can be found online at https://doi.org/10.1016/j.commatsci.2020.109571.

References

[1] A technology roadmap for generation IV nuclear energy systems, Issued by the U.S. DOE Nuclear Energy Research Advisory Committee and the Generation IV International Forum, 2002.
[2] M. Rosental, P. Haubenreich, R. Briggs, The development status of molten-salt breeder reactors, ORNL/TM-4812, (1972) 196–211.
[3] ThorCon power, ThorCon. http://thorconpower.com/, 2019 (accessed 19 September 2019).
[4] D.Q. Xia, C.L. Ren, W. Zhang, H. Han, C.B. Wang, X. Zhang, C. Cheng, P. Huai, Theoretical study of the interaction between metallic fission products and defective graphite, Comput. Mater. Sci. 106 (2015) 129–134, https://doi.org/10.1016/j.commatsci.2015.04.029.
[5] H.E. McCoy, Intergranular cracking of structural materials exposed to fuel salt, ORNL/TM-4782, (1972) 128–136.
[6] J.R.Keiser, Status of tellurium-Hastelloy N studies in molten fluoride salts, ORNL/TM-6002, (1977) 1–23.
[7] L. Lu, Y. Jia, X.-X. Ye, M. Luo, F. Song, Y. Huang, X. Zhou, Z. Li, Z. Jiang, Local structure study of tellurium corrosion of nickel alloy by X-ray absorption spectroscopy, Corros. Sci. 108 (2016) 169–172, https://doi.org/10.1016/j.corsci.2016.03.006.
[8] H.E. McCoy, Status material development for molten salt reactions, ORNL/TM-5920, (1978) 5-6.
[9] M. Vsianska, M. Sob, The effect of segregated sp-impurities on grain-boundary and surface structure, magnetism and embrittlement in nickel, Prog. Mater. Sci. 56 (2011) 817–840, https://doi.org/10.1016/j.pmatsci.2011.01.008.
[10] Y. He, Y. Li, C. Chen, H. Yu, Diffusion coefficient of hydrogen interstitial atom in alpha-Fe, gamma-Fe and epsilon-Fe crystals by first-principle calculations, Int. J. Hydrogen Energy 42 (2017) 27438–27445, https://doi.org/10.1016/j.ijhydene.2017.08.212.
[11] M.A. Tschopp, F. Gao, K.N. Solanki, He-V cluster nucleation and growth in alpha-Fe grain boundaries, Acta Mater. 124 (2017) 544–555, https://doi.org/10.1016/j.actamat.2016.11.027.
[12] X. Li, P. Wu, R. Yang, D. Yan, S. Chen, S. Zhang, N. Chen, Boron diffusion in bcc-Fe studied by first-principles calculations, Chin. Phys. B 25 (2016) 036601, https://doi.org/10.1088/1674-1056/25/3/036601.
[13] D.E. Jiang, E.A. Carter, Carbon dissolution and diffusion in ferrite and austenite from first principles, Phys. Rev. B 67 (2003) 24103, https://doi.org/10.1103/PhysRevB.67.214103.
[14] D. Chen, F. Gao, W.Y. Hu, S.Y. Hu, D. Terentyev, X. Sun, H.L. Heinisch, C.H. Henager, M.A. Khaleel, Migration of Cr-vacancy clusters and interstitial Cr in alpha-Fe using the dimer method, Phys. Rev. B 81 (2010) 064101, https://doi.org/10.1103/PhysRevB.81.064101.
[15] H.H. Xiong, L. Gan, Z.F. Tong, H.H. Zhang, Y. Zhou, Investigation of iron adsorption on composite transition metal carbides in steel by first-principles calculation, J. Phys. Chem. Solids 116 (2018) 30–36, https://doi.org/10.1016/j.jpcs.2018.01.013.
[16] H. Wu, T. Mayeshiba, D. Morgan, High-throughput ab-initio dilute solute diffusion database, Sci. Data 3 (2016) 160054, https://doi.org/10.1038/sdata.2016.54.
[17] X. Wang, X.H. Yu, J. Rong, X.Y. Li, Y. Zhong, J. Feng, Z.L. Zhan, The diffusion behavior of Ti atoms in pure nanocrystalline Fe by first principles calculations, Mater. Res. Express 5 (2018) 095010, https://doi.org/10.1088/2053-1591/aad605.
[18] J.J. Wang, X.G. Lu, N.Q. Zhu, W.S. Zheng, Thermodynamic and diffusion kinetic studies of the Fe-Co system, CALPHAD: Comput. Coupl. Phase Diagrams Thermochem. 58 (2017) 82–100, https://doi.org/10.1016/j.calphad.2017.06.001.
[19] T. Ohnuma, Surface diffusion of Fe and Cu on Fe (001) under electric field using first-principles calculations, Microsc. Microanal. 25 (2019) 547–553, https://doi.org/10.1017/s1431927618015738.
[20] K. Hirata, S. Iikubo, H. Ohtani, First-principles calculations of the effects of Mn, Cr, and Ni on hydrogen diffusion in bcc, fcc, and hcp Fe, Tetsu to Hagane 105 (2019) 109–117, https://doi.org/10.2355/tetsutohagane.TETSU-2018-070.
[21] T.P.C. Klaver, D.J. Hepburn, G.J. Ackland, Defect and solute properties in dilute Fe-Cr-Ni austenitic alloys from first principles, Phys. Rev. B 85 (2012) 174111, https://doi.org/10.1103/PhysRevB.85.174111.
[22] C.Y. Wang, H. Han, D. Wickramaratne, W. Zhang, H. Wang, X.X. Ye, Y.L. Guo, K. Shao, P. Huai, Diffusion of tellurium at nickel grain boundaries: a first-principles study, RSC Adv. 7 (2017) 8421–8428, https://doi.org/10.1039/c6ra28435c.
[23] W. Liu, H. Han, C. Ren, X. He, Y. Jia, S. Wang, W. Zhang, Z. Li, X. Zhou, Y. Zou, P. Huai, H. Xu, First-principles study of intergranular embrittlement induced by Te in the Ni Sigma 5 grain boundary, Comput. Mater. Sci. 88 (2014) 22–27, https://doi.org/10.1016/j.commatsci.2014.02.038.
[24] Y.Y. Jia, H.W. Cheng, J. Qiu, F.F. Han, Y. Zou, Z.J. Li, X.T. Zhou, H.J. Xu, Effect of temperature on diffusion behavior of Te into nickel, J. Nucl. Mater. 441 (2013) 372–379, https://doi.org/10.1016/j.jnucmat.2013.06.025.
[25] G. Kresse, J. Hafner, Abinitio molecular-dynamics for liquid-metals, Phys. Rev. B 47 (1993) 558–561, https://doi.org/10.1103/PhysRevB.47.558.
[26] G. Kresse, J. Hafner, Ab-initio molecular-dynamics simulation of the liquid-metal amorphous-semiconductor transition in germanium, Phys. Rev. B 49 (1994) 14251–14269, https://doi.org/10.1103/PhysRevB.49.14251.
[27] G. Kresse, J. Furthmuller, Efficient iterative schemes for ab initio total-energy calculations using a plane-wave basis set, Phys. Rev. B 54 (1996) 11169–11186, https://doi.org/10.1103/PhysRevB.54.11169.
[28] G. Kresse, D. Joubert, From ultrasoft pseudopotentials to the projector augmented-wave method, Phys. Rev. B 59 (1999) 1758–1775, https://doi.org/10.1103/PhysRevB.59.1758.
[29] J.P. Perdew, K. Burke, M. Ernzerhof, Generalized gradient approximation made simple, Phys. Rev. Lett. 77 (1996) 3865–3868, https://doi.org/10.1103/PhysRevLett.77.3865.
[30] G. Henkelman, B.P. Uberuaga, H. Jonsson, A climbing image nudged elastic band method for finding saddle points and minimum energy paths, J. Chem. Phys. 113 (2000) 9901–9904, https://doi.org/10.1063/1.1329672.
[31] H.J. Monkhorst, J.D. Pack, Special points for brillouin-zone integrations, Phys. Rev. B 13 (1976) 5188–5192, https://doi.org/10.1103/PhysRevB.13.5188.
[32] C.D. Versteylen, N.H. van Dijk, M.H.F. Sluiter, First-principles analysis of solute diffusion in dilute bcc Fe-X alloys, Phys. Rev. B 96 (2017) 094105, https://doi.org/

10.1103/PhysRevB.96.094105.
[33] X. Zhang, T. Hickel, J. Rogal, S. Faehler, R. Drautz, J. Neugebauer, Structural transformations among austenite, ferrite and cementite in Fe-C alloys: a unified theory based on ab initio simulations, Acta Mater. 99 (2015) 281–289, https://doi.org/10.1016/j.actamat.2015.07.075.
[34] C. Kittle, Introduction to Solid State Physics, fifth ed., Wiley, New York, 1996.
[35] Y. Tateyama, T. Ohno, Stability and clusterization of hydrogen-vacancy complexes in alpha-Fe: an ab initio study, Phys. Rev. B 67 (2003) 174105, https://doi.org/10.1103/PhysRevB.67.174105.
[36] A. Jain, S. Ong, G. Hautier, W. Chen, W. Richards, S. Dacek, et al., The materials project: a materials genome approach to accelerating materials innovation, APL Mater. 1 (2013) 011002, https://doi.org/10.1063/1.4812323.
[37] S. Arrhenius, On the reaction rate of the inversion of nonrefined sugar upon souring, J Phys. Chem. 4 (1889) 226–248.
[38] A.D. Le Claire, Solvent self-diffusion in dilute b.c.c. solid solutions, Philos. Mag. 21 (1970) 819–832, https://doi.org/10.1080/14786437008238468.
[39] M.J. Jones, A.D. Le Claire, Solvent self-diffusion in dilute b.c.c solid solutions II. Calculation of Partial Correlation Factors, Philos. Mag. 26 (1972) 1191–1204, https://doi.org/10.1080/14786437208227373.
[40] H. Eyring, The activated complex in chemical reactions, J. Chem. Phys. 3 (1935) 107–115, https://doi.org/10.1063/1.1749604.
[41] G.H. Vineyard, Frequency factors and isotope effects in solid state rate processes, J. Phys. Chem. Solids 3 (1957) 121–127, https://doi.org/10.1016/0022-3697(57)90059-8.
[42] D. Murali, B.K. Panigrahi, M.C. Valsakumar, C.S. Sundar, Diffusion of Y and Ti/Zr in bcc iron: a first principles study, J. Nucl. Mater. 419 (2011) 208–212, https://doi.org/10.1016/j.jnucmat.2011.05.018.
[43] L. Messina, M. Nastar, T. Garnier, C. Domain, P. Olsson, Exact ab initio transport coefficients in bcc Fe-X (X = Cr, Cu, Mn, Ni, P, Si) dilute alloys, Phys. Rev. B 90 (2014) 104203, https://doi.org/10.1103/PhysRevB.90.104203.
[44] C. Domain, C.S. Becquart, Diffusion of phosphorus in alpha-Fe: An ab initio study, Phys. Rev. B 71 (2005) 214109, https://doi.org/10.1103/PhysRevB.71.214109.
[45] S.Y. Huang, D.L. Worthington, M. Asta, V. Ozolins, G. Ghosh, P.K. Liaw, Calculation of impurity diffusivities in alpha-Fe using first-principles methods, Acta Mater. 58 (2010) 1982–1993, https://doi.org/10.1016/j.actamat.2009.11.041.
[46] P.A. Korzhavyi, I.A. Abrikosov, B. Johansson, A.V. Ruban, H.L. Skriver, First-principles calculations of the vacancy formation energy in transition and noble metals, Phys. Rev. B 59 (1999) 11693–11703, https://doi.org/10.1103/PhysRevB.59.11693.
[47] L. Deschepper, D. Segers, L. Dorikensvanpraet, M. Dorikens, G. Knuyt, L.M. Stals, P. Moser, Positron-annihilation on pure and carbon-doped alpha-iron in thermal-equilibrium, Phys. Rev. B 27 (1983) 5257–5269, https://doi.org/10.1103/PhysRevB.27.5257.
[48] C. Zhang, J. Fu, R.H. Li, P.B. Zhang, J.J. Zhao, C. Dong, Solute/impurity diffusivities in bcc Fe: a first-principles study, J. Nucl. Mater. 455 (2014) 354–359, https://doi.org/10.1016/j.jnucmat.2014.07.011.
[49] R.J. Borg, D.Y.F. Lai, The diffusion of gold, nickel, and cobalt in alpha iron: A study of the effect of ferromagnetism upon diffusion, Acta Metall. 11 (1963) 861–866, https://doi.org/10.1016/0001-6160(63)90055-5.
[50] G. Hettich, H. Mehrer, K.M.J.S. Metallurgica, Self-diffusion in ferromagnetic α-iron, Scr. Metall. 11 (1977) 795–802, https://doi.org/10.1016/0036-9748(77)90078-3.
[51] Y. Iijima, K. Kimura, K. Hirano, Self-diffusion and isotope effect in α-iron, Acta Metall. 36 (1988) 2811–2820, https://doi.org/10.1016/0001-6160(88)90127-7.
[52] M. Lubbehusen, H. Mehrer, Self-diffusion in alpha-iron: the influence of dislocations and the effect of the magnetic phase transition, Acta Metall. Mater. 38 (1990) 283–292, https://doi.org/10.1016/0956-7151(90)90058-O.
[53] C.R. Fu, X.F. Zhang, Y.R. Duan, X.Y. Dai, T. Li, Y.J. Xia, Y.Y. Jiang, H. Li, Influence of local surrounding on magnetism in Fe-Ni alloy: a first principles study, J. Magn. Magn. Mater. 492 (2019) 165657, https://doi.org/10.1016/j.jmmm.2019.165657.
[54] R.D. Hatcher, R. Zeller, P.H. Dederichs, Formation entropy and the diffusion constant for vacancies in Cu and alpha-Fe, Phys. Rev. B 19 (1979) 5083–5093, https://doi.org/10.1103/PhysRevB.19.5083.
[55] C.Q. Wang, Y.X. Yang, Y.S. Zhang, Y. Jia, A single vacancy diffusion near a Fe (1 1 0) surface: a molecular dynamics study, Comput. Mater. Sci. 50 (2010) 291–294, https://doi.org/10.1016/j.commatsci.2010.08.017.
[56] D. Kandaskalov, C. Mijoule, D. Connetable, Study of multivacancies in alpha Fe, J. Nucl. Mater. 441 (2013) 168–177, https://doi.org/10.1016/j.jnucmat.2013.05.030.
[57] N. Soneda, T.D. de la Rubia, Defect production, annealing kinetics and damage evolution in alpha-Fe: an atomic-scale computer simulation, Philos. Mag. A 78 (1998) 995–1019.
[58] F. Soisson, C.C. Fu, Cu-precipitation kinetics in alpha-Fe from atomistic simulations: vacancy-trapping effects and Cu-cluster mobility, Phys. Rev. B 76 (2007) 214102, https://doi.org/10.1103/PhysRevB.76.214102.
[59] A. Vehanen, P. Hautojarvi, J. Johansson, J. Ylikauppila, P. Moser, Vacancies and carbon impurities in alpha-iron: Electron irradiation, Phys. Rev. B 25 (1982) 762–780, https://doi.org/10.1103/PhysRevB.25.762.
[60] P. Olsson, C. Domain, J. Wallenius, Ab initio study of Cr interactions with point defects in bcc Fe, Phys. Rev. B 75 (2007) 014110, https://doi.org/10.1103/PhysRevB.75.014110.
[61] P. Olsson, J. Wallenius, C. Domain, K. Nordlund, L. Malerba, Two-band modeling of alpha-prime phase formation in Fe-Cr, Phys. Rev. B 72 (2005) 214119, https://doi.org/10.1103/PhysRevB.72.214119.
[62] M.I. Mendelev, Y. Mishin, Molecular dynamics study of self-diffusion in bcc Fe, Phys. Rev. B 80 (2009) 144111, https://doi.org/10.1103/PhysRevB.80.144111.
[63] A. Seeger, Lattice vacancies in high-purity alpha-iron, Phys. Status Solidi A 167 (1998) 289–311, https://doi.org/10.1002/(sici)1521-396x(199806)167:2<289::Aid-pssa289>3.0.Co;2-v.
[64] A. Inoue, H. Nitta, Y. Iijima, Grain boundary self-diffusion in high purity iron, Acta Mater. 55 (2007) 5910–5916, https://doi.org/10.1016/j.actamat.2007.06.041.
[65] D.W. James, G.M. Leak, Self-diffusion and diffusion of cobalt in alpha and delta-iron, Philos. Mag. 14 (1966) 701, https://doi.org/10.1080/14786436608211966.
[66] C.G. Lee, Y. Iijima, T. Hiratani, K. Hirano, Diffusion of chromium in alpha-iron, Mater. Trans., JIM 31 (1990) 255–261, https://doi.org/10.2320/matertrans1989.31.255.
[67] P. Klugkist, C. Herzig, Tracer diffusion of titanium in alpha-iron, Phys. Status Solidi A 148 (1995) 413–421, https://doi.org/10.1002/pssa.2211480209.
[68] R.C. Robertson, MSRE design and operations report, ORNL/TM-728, (1965) 78.

Supplementary material for

Migration behavior of tellurium in bcc iron against typical alloying elements: a first-principles study

Zheng-De Zhang,[1, 2] Cui-Lan Ren,[1, 3,*] Meng-Lu Tan,[1, 2] Yu-Qi Yang,[2, 4] Ya-Ru Yin,[5] Chang-Ying Wang,[6] Han Han,[1] and Ping Huai[1, 4, 5,*]

[1] *Shanghai Institute of Applied Physics, Chinese Academy of Sciences, Shanghai 201800, China*

[2] *University of Chinese Academy of Sciences, Beijing 100049, China*

[3] *Key Laboratory of Interfacial Physics and Technology, Chinese Academy of Sciences, Shanghai 201800, China*

[4] *Center of Shanghai Light Source, Shanghai Advanced Research Institute, Shanghai 201204, China*

[5] *School of Physical Science and Technology, ShanghaiTech University, Shanghai 201210, China*

[6] *Changzhou Institute of Technology, Changzhou 213032, China*

***Corresponding authors.**

Professor., Ph.D.; Tel/Fax: +86 21 33512449

E-mail address: rencuilan@sinap.ac.cn (Cui-Lan Ren)

Professor., Ph.D., Tel/Fax: +86 21 20685546

E-mail address: huaiping@sinap.ac.cn (Ping Huai)

Note. 1 Pre-factor D_0 and activation energy Q

According to previous literature [1, 2]

$$\mathrm{D} = a_0^2 f_2 C_v \omega_2 \exp\left(-{}^{\mathrm{G}_b}/_{k_B T}\right) \tag{S1}$$

The a_0 is the lattice constant and f_2 is the correlation factor for solute atom, for self-diffusion, the correlation factor denoted as f_0.

The vacancy concentration C_v in thermal equilibrium is defined as:

$$C_v = exp\left(-\frac{G_f}{k_B T}\right) = exp\left(\frac{\Delta S_f}{k_B}\right) exp\left(-\frac{H_f}{k_B T}\right) \tag{S2}$$

The jump frequency of solute-vacancy exchange is described by Eyring's [3] reaction rate theory:

$$\omega = v^* exp\left(-{}^{E_m}/_{k_B T}\right) \tag{S3}$$

where ω_2 denotes the jump frequency of solute atom. v^* is the effective frequency. E_m is the diffusion barrier.

The binding free energy of solute-vacancy ΔG_b is calculated in terms of the binding enthalpy H_b and entropy ΔS_b.

$$G_b = H_b - T\Delta S_b \tag{S4}$$

$$\exp\left(-{}^{\mathrm{G}_b}/_{k_B T}\right) = \exp(\frac{\Delta S_b}{k_B})\exp(-\frac{H_b}{k_B T}) \tag{S5}$$

Hence,

$$\mathrm{D} = a_0^2 f_2 v_2^* exp\left(\frac{\Delta S_f + \Delta S_b}{k_B}\right) exp\left(-\frac{E_m + H_f + H_b}{k_B T}\right) \tag{S6}$$

Compared to the Arrhenius equation

$$D = D_0 exp(-\frac{Q}{k_B T}) \tag{S7}$$

We have

$$\mathrm{Q} = H_f + H_b + E_m \tag{S8}$$

$$D_0 = a_0^2 f v^* \exp\left(\frac{\Delta S_f + \Delta S_b}{k_B}\right) \tag{S9}$$

For self-diffusion of iron, $H_b = 0,\ \Delta S_b = 0$.

Note. 2 Vacancy formation entropy ΔS_f

According to previous literature[4], the vacancy formation entropy is written as following:

$$\Delta S_f = \left[\sum_{i=1}^{3N-3} \ln\left(\frac{k_B T}{h v_i^{vac}}\right) - \frac{N-1}{N}\sum_{i=1}^{3N} \ln\left(\frac{k_B T}{h v_i^{pure}}\right)\right] k_B \quad \text{(S10)}$$

where v_i^{pure} is the vibrational frequencies in three degrees of freedom of the atoms in pure bcc lattice and v_i^{vac} is the frequencies of the atoms in the system containing one vacancy.

Unfold the Eq. (S10)

$$\Delta S_f = \left[ln\left(\frac{k_B T}{h}\right)^{3N-3} + ln\left(\frac{1}{v_1^{vac} v_2^{vac} \cdots v_{3N-3}^{vac}}\right) - \frac{N-1}{N} ln\left(\frac{k_B T}{h}\right)^{3N} - \frac{N-1}{N} ln\left(\frac{1}{v_1^{pure} v_2^{pure} \cdots v_{3N}^{pure}}\right)\right] k_B$$

$$= \left[\ln \frac{\left(v_1^{pure} v_2^{pure} \cdots v_{3N-3}^{pure} v_{3N-2}^{pure} v_{3N-1}^{pure} v_{3N}^{pure}\right)^{\frac{N-1}{N}}}{v_1^{vac} v_2^{vac} \cdots v_{3N-3}^{vac}}\right] k_B \quad \text{(S11)}$$

For pure bcc lattice, the vibrational frequencies of all atoms are the same. Generally, the vacancy affects the vibration of its first nearest neighbor (1NN) and second nearest neighbor (2NN) atoms, for which there are eight 1NN sites and twelve 2NN sites for each site in bcc lattices. By considering the symmetry, the only the 1NN and 2NN sites (N=8+12+1=21) are simplified selected to calculate the vibration frequency. Thus, Eq. (S11) can be written as:

$$\Delta S_f = \left[ln \frac{\left(\left(v_1^{pure} v_2^{pure} v_3^{pure}\right)^{21}\right)^{\frac{21-1}{21}}}{\left(v_1^{vac,1NN} v_2^{vac,1NN} v_3^{vac,1NN}\right)^8 \left(v_1^{vac,2NN} v_2^{vac,2NN} v_3^{vac,2NN}\right)^{12}}\right] k_B$$

$$= \left[ln \frac{\left(\prod_1^3 v_i^{pure}\right)^{20}}{\left(\prod_1^3 v_i^{vac,1NN}\right)^8 \left(\prod_1^3 v_i^{vac,2NN}\right)^{12}}\right] k_B \quad \text{(S12)}$$

where v_i^{pure} is the vibrational frequencies in three degrees of freedom of one iron atom in pure bcc iron. $v_i^{vac,1NN}$ and $v_i^{vac,2NN}$ are the frequencies of the 1NN and 2NN iron atom to the vacancy in the system containing one vacancy.

Note. 3 Solute-vacancy binding entropy ΔS_b for bcc lattice

According to previous literature[2], the binding entropy is written as following:

$$\Delta S_b = \left[\sum_{i=1}^{3N-3} ln\left(\frac{v_i^{vac}}{v_i^{vac,sol}}\right) + \sum_{i=1}^{3N} ln\left(\frac{v_i^{sol}}{v_i^{pure}}\right)\right] k_B$$

$$= \left[ln\frac{(v_1^{vac}v_2^{vac}\cdots v_{3N-3}^{vac})(v_1^{sol}v_2^{sol}\cdots v_{3N}^{sol})}{(v_1^{pure}v_2^{pure}\cdots v_{3N}^{pure})(v_1^{vac,sol}v_2^{vac,sol}\cdots v_{3N-3}^{vac,sol})}\right] k_B \quad \text{(S13)}$$

By considering the vacancy generally affect the vibration of the eight 1NN atoms, N=8+1=9 is selected here. Among the eight 1NN sites adjacent to vacancy, there are one solute atom, three 2NN host atoms relative to the solute atom, three 3NN host atoms relative to the solute atom and one 5NN host atom relative to the solute atom. Hence, we have:

$$\Delta S_b = \left[ln\frac{(\Pi_1^3 v_i^{vac})^8(\Pi_1^3 v_i^{sol})(\Pi_1^3 v_i^{sol,1NN})(\Pi_1^3 v_i^{sol,2NN})^3(\Pi_1^3 v_i^{sol,3NN})^3(\Pi_1^3 v_i^{sol,5NN})}{(\Pi_1^3 v_i^{pure})^9(\Pi_1^3 v_i^{vac,sol})(\Pi_1^3 v_i^{vac,sol,2NN})^3(\Pi_1^3 v_i^{vac,sol,3NN})^3(\Pi_1^3 v_i^{vac,sol,5NN})}\right] k_B \text{ (S14)}$$

Note. 4 Migration energy profiles for solutes in bcc iron

The minimum energy paths and their corresponding energy barriers of solutes (Te, Cr, Mo, Nb, Ti, Al, Co, Cu, Mn, Ni, V and W) in nine-frequency model for bcc iron lattice.

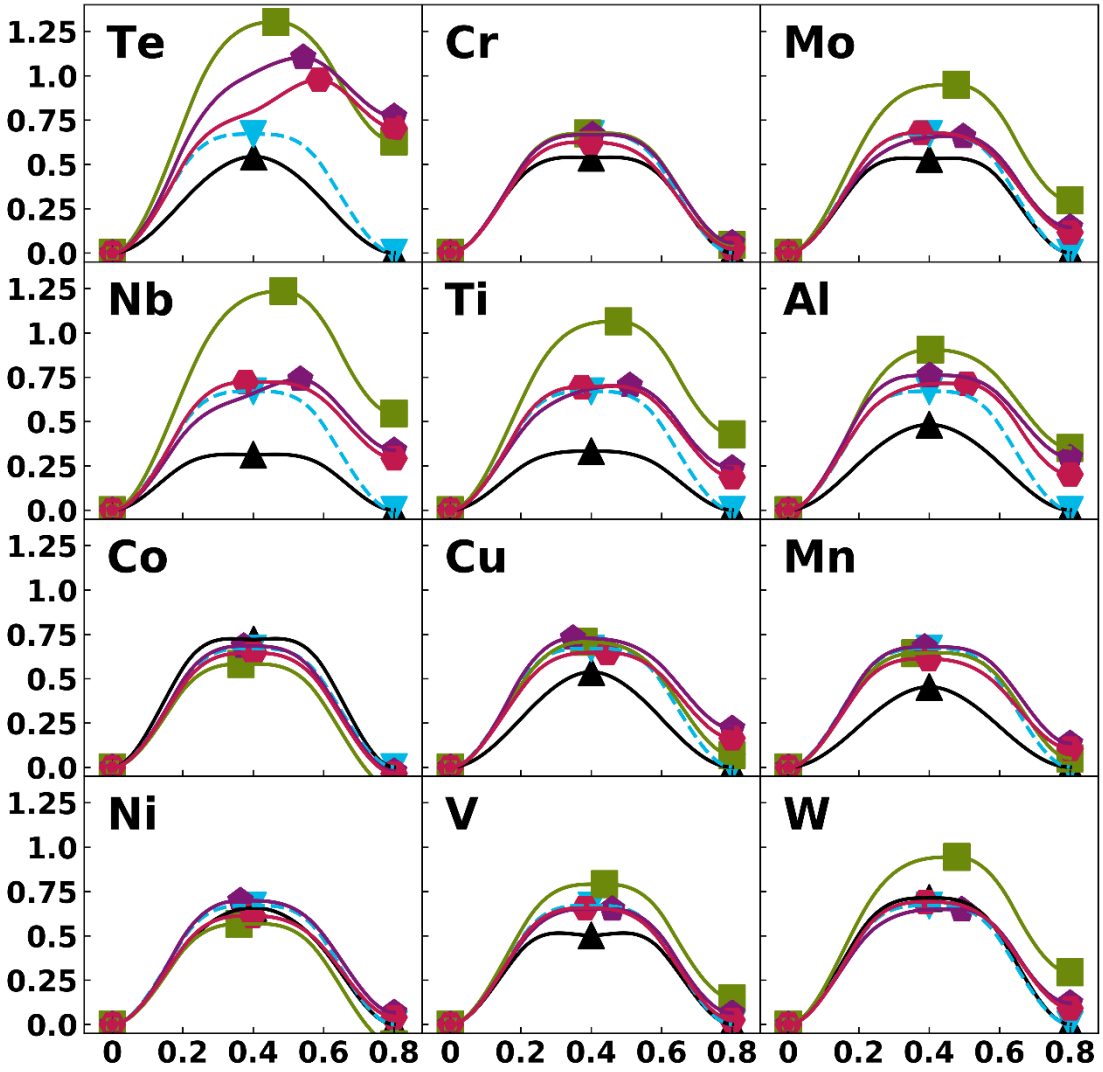

Fig. S1. The energy profiles for lattice diffusions in various solute-doped iron.

Table. S1

The corresponding migration barriers and effective frequencies for the solutes migration processes in Fig. S1.

		ω_0	ω_2	ω_3	ω_3'	ω_3''	ω_5	ω_4	ω_4'	ω_4''	ω_6	ω_{2nn}
E_m	Fe	0.67										2.59
(eV)		0.69[a], 0.65[b], 0.67[c], 0.55[d]										
	Te		0.54	1.30	1.10	0.97	0.69	0.67	0.33	0.27	0.50	2.28
	Cr		0.54	0.67	0.67	0.62	0.72	0.63	0.61	0.60	0.68	2.34
			0.56[a]	0.69[a]	0.68[a]	0.64[a]	0.72[a]	0.65[a]	0.62[a]	0.61[a]	0.69[a]	
	Mo		0.53	0.95	0.66	0.68	0.65	0.65	0.51	0.56	0.77	2.04
	Nb		0.31	1.24	0.62	0.72	0.62	0.70	0.28	0.43	0.78	1.57
	Ti		0.38	1.06	0.70	0.69	0.62	0.63	0.46	0.50	0.79	1.62
	Al		0.48	0.90	0.76	0.71	0.63	0.55	0.46	0.51	0.61	2.56
	Co		0.72	0.58	0.68	0.65	0.72	0.70	0.70	0.68	0.62	2.88
	Cu		0.54	0.71	0.73	0.65	0.72	0.64	0.51	0.48	0.54	2.87
	Mn		0.45	0.64	0.68	0.61	0.74	0.59	0.55	0.50	0.62	2.52
	Ni		0.66	0.57	0.70	0.61	0.78	0.68	0.63	0.57	0.56	3.01
	W		0.71	0.94	0.65	0.69	0.65	0.65	0.52	0.60	0.78	2.50
v^*	Fe	4.67										5.85
(THz)		4.65[a], 6[e], 4.9[f]										
	Te		2.97	5.07	5.49	5.80	4.90	4.39	4.64	5.22	4.55	3.09
	Cr		4.95	4.88	4.53	4.51	4.63	4.55	4.36	4.41	4.70	7.10
			5.03[a]	4.92[a]	4.58[a]	4.57[a]	4.70[a]	4.59[a]	4.38[a]	4.44[a]	4.64[a]	
	Mo		4.61	5.13	4.88	4.69	4.68	4.69	4.85	4.46	4.71	6.12
	Nb		4.14	5.28	5.05	4.77	4.77	4.66	4.91	4.32	4.70	5.28
	Ti		5.09	5.32	4.87	4.73	4.73	4.60	4.67	4.42	4.69	7.65
	Al		5.34	4.83	4.69	4.91	4.64	4.13	4.22	5.21	4.39	6.63
	Co		4.53	4.48	4.64	4.55	4.70	4.65	4.65	4.68	4.64	5.30
	Cu		3.27	4.45	4.81	4.53	4.85	4.41	4.37	4.72	4.48	4.57
	Mn		4.37	4.75	4.54	4.43	4.78	4.59	4.37	4.34	4.66	6.07
	Ni		4.15	4.43	4.69	4.47	4.87	4.70	4.59	4.61	4.62	4.77
	W		3.48	5.00	4.85	4.66	4.67	4.70	4.90	4.55	4.74	4.19

[a] DFT result from Wu. 2016. [5]

[b] DFT result from Murali. 2011. [6]

[c] DFT result from Soisson. 2007. [7]

[d] Experimental data from Vehanen. 1982. [8]

[e] DFT result from Messina. 2014. [9]

[f] DFT result from Domain. 2005. [10]

Note. 5 The energy profiles for long distance diffusion via solute-V_2 cluster.

The minimum energy paths of long-term migration of solute-V_2 cluster. The solutes including Te, Cr, Mo, Nb, Ti, Al, Co, Cu, Mn, Ni, V and W are considered here. The values in the figure are the maximal energy barriers for the solutes over the designed net diffusions.

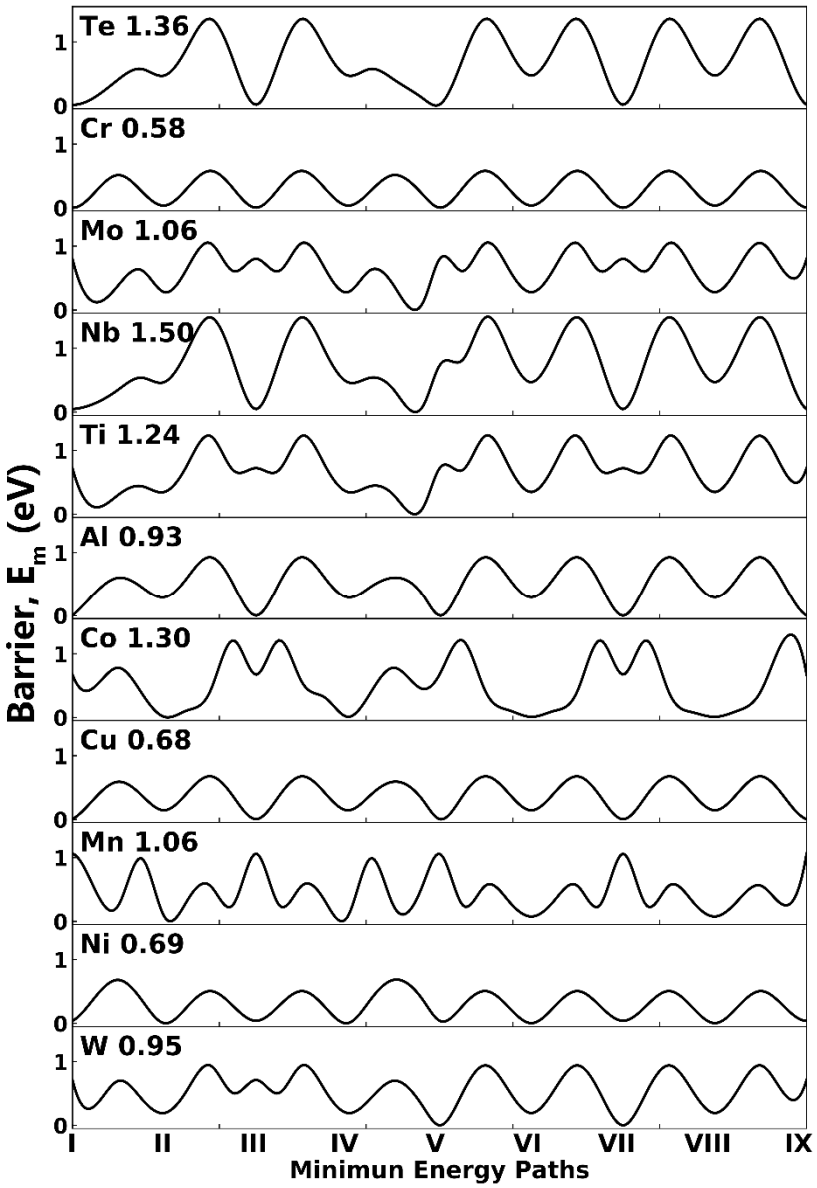

Fig. S2. Energy profiles for long distance solute diffusion via solute-V_2 cluster in α-Fe and corresponding maximum barriers.

References

[1] M. Mantina, Y. Wang, L.Q. Chen, Z.K. Liu, C. Wolverton, First principles impurity diffusion coefficients, Acta Mater., 57 (2009) 4102-4108. https://doi.org/10.1016/j.actamat.2009.05.006.

[2] H.Y. Wang, X.Y. Gao, H.P. Ren, S.M. Chen, Z.F. Yao, Diffusion coefficients of rare earth elements in fcc Fe: A first-principles study, J. Phys. Chem. Solids, 112 (2018) 153-157. https://doi.org/10.1016/j.jpcs.2017.09.025.

[3] H. Eyring, The activated complex in chemical reactions, J. Chem. Phys., 3 (1935) 107-115. https://doi.org/10.1063/1.1749604.

[4] S.Y. Huang, D.L. Worthington, M. Asta, V. Ozolins, G. Ghosh, P.K. Liaw, Calculation of impurity diffusivities in alpha-Fe using first-principles methods, Acta Mater., 58 (2010) 1982-1993. https://doi.org/10.1016/j.actamat.2009.11.041.

[5] H. Wu, T. Mayeshiba, D. Morgan, High-throughput ab-initio dilute solute diffusion database, Sci. Data, 3 (2016). https://doi.org/10.1038/sdata.2016.54.

[6] D. Murali, B.K. Panigrahi, M.C. Valsakumar, C.S. Sundar, Diffusion of Y and Ti/Zr in bcc iron: A first principles study, J. Nucl. Mater., 419 (2011) 208-212. https://doi.org/10.1016/j.jnucmat.2011.05.018.

[7] F. Soisson, C.C. Fu, Cu-precipitation kinetics in alpha-Fe from atomistic simulations: Vacancy-trapping effects and Cu-cluster mobility, Phys. Rev. B, 76 (2007). https://doi.org/10.1103/PhysRevB.76.214102.

[8] A. Vehanen, P. Hautojarvi, J. Johansson, J. Ylikauppila, P. Moser, Vacancies and carbon impurities in alpha-iron - electron-irradiation, Phys. Rev. B, 25 (1982) 762-780. https://doi.org/10.1103/PhysRevB.25.762.

[9] L. Messina, M. Nastar, T. Garnier, C. Domain, P. Olsson, Exact ab initio transport coefficients in bcc Fe-X (X=Cr, Cu, Mn, Ni, P, Si) dilute alloys, Phys. Rev. B, 90 (2014). https://doi.org/10.1103/PhysRevB.90.104203.

[10] C. Domain, C.S. Becquart, Diffusion of phosphorus in alpha-Fe: An ab initio study, Phys. Rev. B, 71 (2005). https://doi.org/10.1103/PhysRevB.71.214109.